

Assessing the effects of atmospheric stability on the fine structure of surface layer turbulence using local and global multiscale approaches

Bin Shi^{a)} and Brani Vidakovic^{b)}

School of Industrial and Systems Engineering, Georgia Institute of Technology, Atlanta, Georgia 30332-0205

Gabriel G. Katul^{c)}

Nicholas School of the Environment and Earth Sciences, Duke University, P.O. Box 90328, Durham, North Carolina 27708-0328

John D. Albertson^{d)}

Department of Civil and Environmental Engineering, Duke University, Durham, North Carolina 27708-0328

(Received 9 December 2004; accepted 18 February 2005; published online 26 April 2005)

The conceptual framework for modeling the inertial subrange is strongly influenced by the Richardson cascade, now the subject of various reinterpretations. One apparent departure from the Richardson cascade is attributed to boundary conditions influencing large-scale motion, which in turn, can directly interact with smaller scales thereby destroying the universal statistical scaling attributes of the inertial subrange. Investigating whether boundary conditions and inertial subrange eddies interact continues to be an active research problem in contemporary turbulence research. Using longitudinal u , lateral v , and vertical w velocities colocated with temperature T time series measurements collected in the atmospheric surface layer, we evaluate whether the inertial subrange is influenced by different stability regimes. The different stability regimes are proxies for different boundary conditions, as upper boundary condition forces the mechanical shear and lower boundary condition forces the surface heating and buoyancy. The novelty of the present work lies in its combined use of global and local scaling properties (e.g., quasi-Hurst exponent, distributional properties of the wavelet coefficients, and Tsallis's thermodynamic entropy measures) to assess whether atmospheric stability impacts both local and global inertial subrange scaling for velocity and temperature. © 2005 American Institute of Physics. [DOI: 10.1063/1.1897008]

I. INTRODUCTION

The structure of turbulence in the inertial subrange has received much research attention over the past 50 years.¹ This strong interest is attributed to the possible emergence of universal or quasiuniversal theories of turbulence,²⁻⁵ which is a research area of interest in many fields (including finance). The inertial subrange encompasses eddies much larger than the viscous dissipation scales yet much smaller than the integral length scale L_I of the flow. The basic premise for the emergence of universal scaling is that large-scale anisotropic forcing characteristics (i.e., boundary effect conditions) are lost during the Richardson cascade process, thereby achieving local isotropy and universality at sufficiently smaller inertial scales.⁶ However, several experiments and simulations over the past two decades suggest persistent effects of large-scale anisotropies at these so-called inertial scales, even for very high Reynolds numbers and after many cascading steps.⁷ The departure from the so-called Kolmogorov⁸ view of universal scaling and subsequent

refinements⁹ is now supported by numerous observations and theoretical arguments regarding the anomalous scaling in measured structure functions, particularly for passive scalars,^{3,7,10-12} and static pressure.¹³ The anomalous scaling is commonly attributed to short circuiting of the energy cascade process due to the existence of organized large-scale features such as ramplike structures, which are influenced by boundary conditions, and themselves directly influence small-scale turbulence.^{7,14} Several theoretical arguments have been put forth to explain the apparent departure between experiments and K41. For example, Qian (Refs. 15 and 16) demonstrated that (1) K41 scaling can only be attained at infinite Reynolds number ($R_\lambda = \lambda \times \sigma_u / \nu$, where λ is the Taylor microscale, σ_u is the longitudinal velocity standard deviation, and ν is the kinematic viscosity), (2) the effects of finite R_λ on the structure function statistics decay slowly with increasing R_λ (e.g., Qian's work demonstrated that the decay is on the order of $R_\lambda^{-\mu}$ for third-order structure function and $\mu \leq 6/5$), and (3) the energy injection mechanism may be important. Recently, Gagne *et al.*¹⁷ indirectly confirmed all three findings experimentally using data collected for different flow types (i.e., different injection mechanism) and different R_λ .

Hence, it is clear that in addition to R_λ , surface heating

^{a)}Electronic mail: bshi@isye.gatech.edu

^{b)}Electronic mail: brani@isye.gatech.edu

^{c)}Electronic mail: gaby@duke.edu

^{d)}Electronic mail: john.albertson@duke.edu

(or cooling), and thereby atmospheric stability class, can be responsible for differences in kinetic energy injection (or removal in the case of stable flows) mechanism, thereby, introducing significant departure from K41.

To quantify whether boundary conditions (or energy injection mechanism) influence the statistical properties of the fine scale structure of the atmospheric surface layer, we utilize two methods: (i) a global scaling self-similarity index, and (ii) a scalewise evolution of nonparametric estimates of probability densities in the wavelet domain. Each of these measures will be applied to turbulence time series measurements collected for three atmospheric stability regimes: unstable, near-neutral, and stable stratifications. An analysis of variance (ANOVA)-type technique will then be applied to assess the significance of atmospheric stability factors on these two multiscale measures. The main novelty of this work is in utilizing both global and local multiscale measures to assess the effects of atmospheric stability on the statistical structure of the inertial subrange of several flow variables. However, before we describe these multiscale methods, a brief description of the experiment and the data set will be provided.

II. DATA

Time series measurements of longitudinal u , lateral v , and vertical w velocities and air temperature T were collected over a grass surface at the Blackwood Division of the Duke Forest near Durham, North Carolina. The measurements were collected on 12–16 June 1995 at 5.2 m using a Gill triaxial sonic anemometer. The measurements were sampled at $f_s=56$ Hz and were subsequently divided into 19.5 min intervals to produce $N=65\,536$ time measurement per flow variable per run. Our choice of 19.5 min intervals for a run is a compromise between the need for stationary conditions at long time scales and maximizing the statistical sample size within a given run. The experiment resulted in an ensemble of 95 runs over a wide range of atmospheric stability conditions ranging from near convective to stable atmospheric flows.¹⁸ Using the atmospheric surface layer stability parameter, $\xi(=z/L)$, these 95 runs were then classified into one of the three stability classes: stable, near neutral, and unstable. Here, L is the Obukhov length and z is the height from the ground surface. With this classification, six runs were collected in stable stability conditions, 23 runs were collected under near-neutral atmospheric stability conditions, and the rest were collected under unstable atmospheric stability conditions. We then selected six runs from the near neutral class and six runs from the unstable stability class such that the ensemble mean wind speed \bar{U} of these six runs were comparable to those six runs collected under stable atmospheric stability conditions. The scalewise analysis only utilizes these 18 runs while the global analysis makes use of all 95 runs. The wind speed ensemble mean and standard deviations of the six runs for unstable, stable, and neutral conditions are provided in Table I. Further details about the experimental setup, atmospheric stability conditions, the various measures used in the inertial subrange identification,

TABLE I. Mean and standard deviations of the six runs for unstable, stable, and neutral wind speeds.

	Unstable	Neutral	Stable
Mean (\bar{U})	1.8096	1.9782	1.814
Standard (\bar{U})	0.0789	0.2502	0.4678

and instrumentation details can be found elsewhere^{18,19} though we note that R_λ exceeded 10^3 for all runs.¹⁸

III. METHODS OF ANALYSIS

In this section, the methodologies for quantifying the effects of ξ on the local and global scaling properties of the inertial subrange are described. These methods include: (i) zero-crossing analysis to estimate the so-called quasi-Hurst exponent, and (ii) scalewise parameter fitting of exponential power distributions (\mathcal{EPD}) in the wavelet domain. We also show that the latter approach has theoretical links to the well-known Tsallis entropy measure. Linking these empirical exponential power distribution parameter to the Tsallis entropy measure is of interest here given the recent theoretical results that demonstrate how a nonlinear Fokker–Plank equation can reproduce essential features about the inertial cascade via Tsallis entropy.

These analytic tools will be utilized to assess whether ξ affects the inertial subrange. We note that these measures are sensitive to different assumptions; hence, if ξ significantly affects the inertial subrange, it is likely to be resolved by these two methods.

A. Global index: Quasi-Hurst exponent

The Hurst exponent (after British hydrologist Hurst, Ref. 20) is a measure of “roughness” of self-affine time series. There are many methods to estimate the Hurst exponent of a stationary process. The zero-crossing method²¹ is based on counting the number of zero crossings Z_N , producing an estimate of the Hurst exponent given by

$$\hat{H} = \frac{1}{2} \{1 + \log_2(1 \pm |\cos(\pi S_N)|)\}, \quad (1)$$

where $S_N = Z_N/(N-1)$ is an average number of zero crossings for the different time series of length N , and sign \pm (alternatively $-$) in \pm is taken if the true exponent H is above (below) $1/2$. Usually, it is not difficult to decide whether the true exponent H is above or below $1/2$ by observing the time series, unless the true H is close to $1/2$. It was also demonstrated (Ref. 21) that the \hat{H} is asymptotically Gaussian for the fractional Brownian motion (fBm) process when the true Hurst exponent does not exceed $3/4$.

The estimation of \hat{H} via (1) is valid only for time series with stationary increments. For time series lacking stationary increments, as may be the case in turbulence time series measurements, we call \hat{H} the *quasi-Hurst* exponent. One of the attributes distinguishing turbulence signals from fBm is the distinction between the quasi-Hurst and Hurst exponents. Theoretically, the quasi-Hurst and Hurst exponents coincide

for fBm (since fBm has stationary increments). We empirically confirmed this convergence using 1000 fBm paths constructed with a true Hurst exponent of $1/3$. The resulting average \hat{H} is 0.3331 with standard deviation of 0.06. The p value of a t test for the equality of \hat{H} to $1/3$ is 0.9. Such a large p value suggests that the \hat{H} is an adequate estimator of the Hurst exponent for a fBm process. On the other hand, the quasi-Hurst exponent for turbulence time series measurement is quite variable and significantly exceeds $1/3$. This discrepancy may be utilized to diagnose how atmospheric stability alters the global scaling parameter. That is, by analyzing deviations of \hat{H} from $1/3$ (or the Kolmogorov scaling) for turbulence measured under different stability conditions, a logical basis for tracking how ξ impacts global scaling of inertial subrange turbulence can be developed.

B. Local index: Evolutionary models of scalewise empirical densities of wavelet coefficients

Another method for assessing the effects of atmospheric stability on the inertial subrange is the sensitivity of the probability density function (pdf) of the wavelet coefficients of a given flow variable to variations in ξ . It is a case-verified fact that the scalewise distribution of wavelet coefficients appear similar for a variety of signals and images. Typically, their empirical distributions are symmetric with a sharp peak at zero. Guided by this opulent evidence, Mallat²² proposed modelling a “typical” wavelet coefficient X by an exponential power family of distributions, $\mathcal{EPD}(\alpha, \beta)$, having the following pdf:

$$f(x) = K e^{-(|x|/\alpha)^\beta}, \quad (2)$$

where α is the scale parameter, β is the shape parameter, and K is a normalizing constant given by $K = \beta/[2\alpha\Gamma(1/\beta)]$. In the context of wavelet modeling, this approach is often referred to as Mallat’s model and reduces to Gaussian for $\beta = 2$, to double exponential for $\beta = 1$ and trivially to uniform for $\beta = 0$. Hence, by investigating how ξ affects α and β at various scales, we can assess whether atmospheric stability impacts the scalewise wavelet coefficients. Such coefficients, belonging to single scale, can be thought of as independent due to the decorrelation property of discrete wavelet transformations (DWT). To estimate these pdf parameters in $\mathcal{EPD}(\alpha, \beta)$, a moment-matching method is adopted. The method is based on matching the theoretical moments, given by

$$E(|X|) = 2K \frac{\alpha^2 \Gamma\left(\frac{2}{\beta}\right)}{\beta}, \quad E(X^2) = 2K \frac{\alpha^3 \Gamma\left(\frac{3}{\beta}\right)}{\beta} \quad (3)$$

with their empirical counterparts: $1/N \sum |x_i|$ and $1/N \sum x_i^2$. Computation of these estimators is not difficult and involves solving one nonlinear equation, and the empirical counterparts for two quantities in (3) can be readily obtained. While the Mallat distribution model appears arbitrary, we explore in the Appendix its potential relationship with the Tsallis Maxent distribution, now receiving significant attention in turbulence research (e.g., Ref. 23). Beck²³ demonstrated that the scaling properties of high Reynolds number turbulence, in-

cluding the probability densities and scaling exponents can be well described using nonextensive measures.

From the Appendix, we show that Mallat’s model parameters can be related to the nonextensive Tsallis entropy parameters, which themselves are shown (e.g., Ref. 23) to be connected to parameters from a nonlinear Fokker–Plank equation with random frictional force. In particular, we show in the Appendix that when β is assumed from a particular prior, the marginal likelihood obtained from the \mathcal{EPD} model in a Bayesian fashion is the maximum Tsallis entropy solution. Because Mallat’s model parameters can be easily linked to geometric attributes of the wavelet coefficient probability distributions, much of our discussion will focus on the effect of atmospheric stability on Mallat model parameters (scale by scale). However, these model parameters do have an unambiguous physical interpretation within the context of maximum Tsallis entropy distribution.

C. Fitting the fBm to Mallat’s model

We generated 100 independent runs of fBm using the Wood–Chan algorithm and computed their wavelet coefficients. We normalized the coefficients at each scale to have a unit variance and fitted the Mallat model to these normalized coefficients. At each scale, we obtained 100 shape parameters. Finally, we performed the nonparametric ANOVA analysis (Kruskal–Wallis test) to assess whether the scale index affects the shape parameters. We found a high p value ($=0.7180$) that indicates the shape parameter is invariant to scale. This finding is crucial for turbulence data as increased intermittency with scale can be readily measured as scalewise shift in the Mallat shape parameters. To illustrate, we show the fitted \mathcal{EPD} of the scalewise wavelet coefficients for the fBm in Fig. 1. Unlike turbulence, these pdfs are nearly Gaussian at all levels (scales), as theoretically expected.

IV. ATMOSPHERIC STABILITY EFFECTS ON THE INERTIAL SUBRANGE

In this section, we discuss the effects of atmospheric stability on the quasi-Hurst exponent (global scaling) and the parameters of the \mathcal{EPD} distribution (local scaling). As mentioned before, the quasi-Hurst exponent \hat{H} is a global fractal index of a time series. Systematic variability of global scaling property with respect to stability factors can be used as indicator of interactions between boundary conditions and inertial subrange scaling.

For each stability class, a descriptive summary of the quasi-Hurst exponent of the four turbulent flow variables is reported in Table II. These exponents are all calculated by the zero-crossing method. Interestingly, we found that for u and v , the scaling exponents exceed those computed from K41 (i.e., 0.333) and do not vary appreciably with stability class. In fact, the scaling exponents for u and v lead to fractal dimensions (in a monofractal model²) on the order of 2.86. When compared to other intermittency models, these exponents (0.42–0.44) are somewhat higher than predicted by the She–Leveque²⁴ or K62 (Ref. 9) models (0.39) hinting that external effects that are not entirely connected with classical internal intermittency buildup are at play.

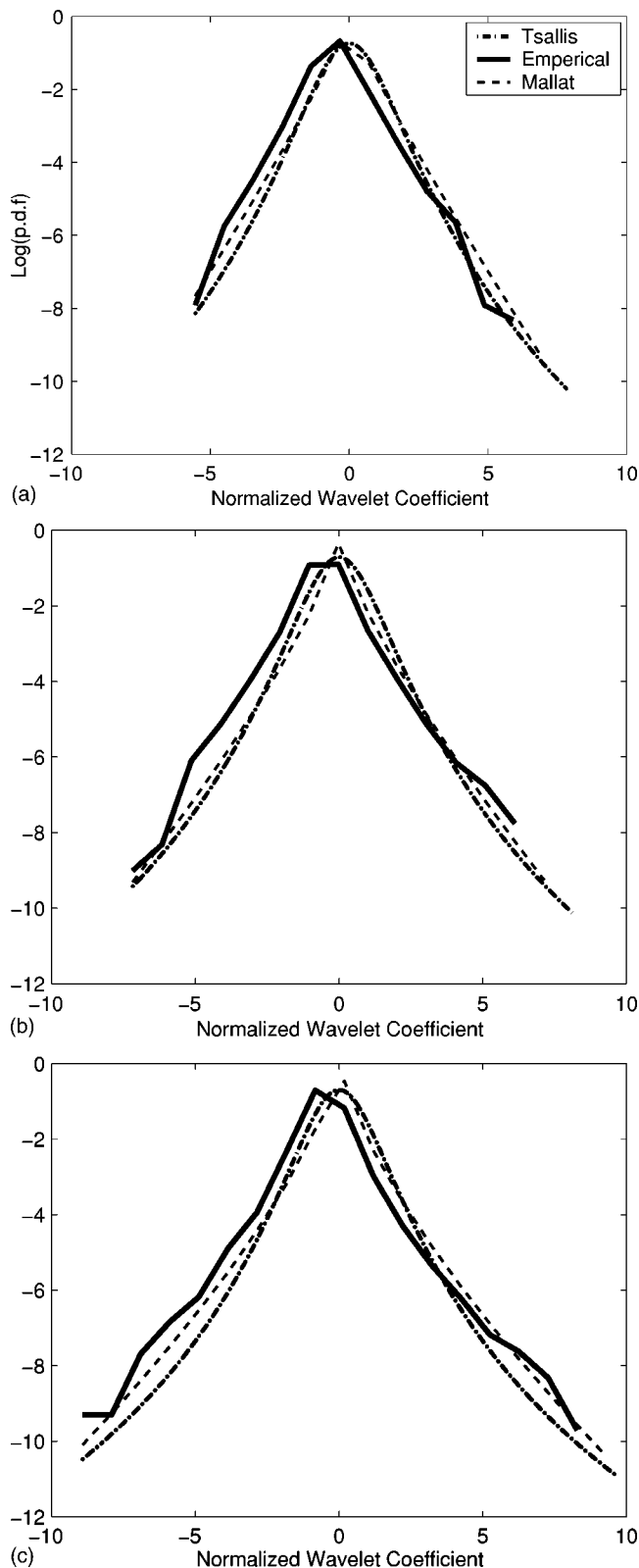


FIG. 1. The comparison between Tsallis Maxent distribution (dash dot), the empirical distribution (dash), and Mallat's model (solid) at the three finest scales of the discrete wavelet transformation. The left panel is the coarsest scale, while the finest scale is at the right panel. The fitted parameters for the three scales are $q=1.3263, 1.3575, 1.3688$, and $\beta=0.8133, 0.6467, 0.5767$, respectively, from the left to the right.

The exponents for the w time series for unstable and stable conditions are bounded by K41 and the She–Leveque (or K62) predictions. Surprisingly, for neutral flows (and for w only), the exponent was lower than K41. The difference between the global exponents for u and w clearly suggests anisotropy not consistent with K41 assumptions.

Upon comparing the global exponents of T and u , we find that the two exponents significantly differ for unstable conditions at the 99% level (using a student t test) but not for near-neutral flows. This analysis lends support to a recent study by Aivalis *et al.* (Ref. 25) who found that for strongly unstable conditions, two scaling ranges emerge in higher order structure functions. One towards the smaller scales, which is the classical inertial range, while the other for larger scales in which the effects of buoyant convective production may still persist. Aivalis *et al.* (Ref. 25) attributed the buoyant-convective scaling to the active role of temperature in the production of turbulent kinetic energy (see also Katul and Parlange²⁶ for further evidence of the active role of temperature using multiple scalars). We note that for stable flows, the u and T global exponents do not differ at the 99% level. This may be attributed to the small number of runs (=6) for statistical significance testing, or alternatively, that the weak removal of turbulent kinetic energy for stable flows is occurring at larger scales than the injection of kinetic energy at near-convective conditions.

We tested the significance of the ANOVA components for the above quasi-Hurst exponents to quantify how the atmospheric stability condition affects the global fractal geometry of each variable. The results are summarized by the p values, which are used again to test the equality of the quasi-Hurst exponents under three different stability conditions.

It is clear from Table II that the stability does not impact the global scaling of the longitudinal and lateral velocities significantly and this is supported by their relatively large p values (0.22 and 0.16, respectively). Meanwhile, the air temperature and vertical velocity are significantly influenced by atmospheric stability and the corresponding ANOVA test p values are quite small (0.0027 and 0, respectively). Hence, we conclude that atmospheric stability has a statistically discernable effect on the global scaling properties of the inertial subrange of T and w .

We use Mallat's \mathcal{EPD} model in the wavelet domain to further explore this finding at the finest scales. The first step is to determine the pdf parameters of the normalized wavelet coefficients in the \mathcal{EPD} model at each scale. After estimating the parameters for each flow variable, we can assess the significance of atmospheric stability at a specific scale. In this analysis, we restrict the scalewise calculations to the finest 3 (out of 16) detail levels to ensure that these wavelet coefficients fall within the inertial subrange (identified as in Refs. 27 and 28) and ensure minimum distortions due to Taylor's hypothesis.

Both pdf plots (Fig. 2) and Q - Q plots (Fig. 3) show that \mathcal{EPD} model fits well the turbulence measurements. Thus, it is natural to regard the scalewise parameters of this model as local scale indices of turbulence. We estimated these parameters for each of the runs within each stability class and tested their equality across different atmospheric stability

TABLE II. Mean and standard deviations of the quasi-Hurst exponent \hat{H} 's for the four flow variables. The numbers in the brackets are the statistics for the selected six runs for each stability regime described in the experimental setup and are reported here for reference.

Turbulence	\hat{H}	Temperature		u		v		w	
		Mean	Standard	Mean	Standard	Mean	Standard	Mean	Standard
s	Unstable	0.419	0.053	0.444	0.049	0.403	0.051	0.392	0.086
t		(0.417)	(0.043)	(0.446)	(0.026)	(0.404)	(0.045)	(0.328)	(0.032)
a	Neutral	0.457	0.047	0.454	0.028	0.395	0.034	0.2515	0.059
b		(0.431)	(0.044)	(0.449)	(0.040)	(0.399)	(0.060)	(0.285)	(0.095)
i	Stable	0.388	0.052	0.419	0.050	0.437	0.038	0.356	0.045
l		(0.388)	(0.052)	(0.419)	(0.050)	(0.437)	(0.038)	(0.356)	(0.045)
i	All	0.427	0.055	0.446	0.045	0.403	0.047	0.356	0.098
t		(0.412)	(0.047)	(0.438)	(0.040)	(0.413)	(0.049)	(0.323)	(0.067)

classes. The results from this analysis should be taken with caution because the parameter comparisons across stability regimes for a specified scale index j assume that the eddy sizes represented by j are the same irrespective of stability

(here—the larger the j the smaller the turbulent scale). While every effort was made to select the six runs across different stability classes with comparable mean wind speeds, the distortions due to Taylor's hypothesis may be dependent on

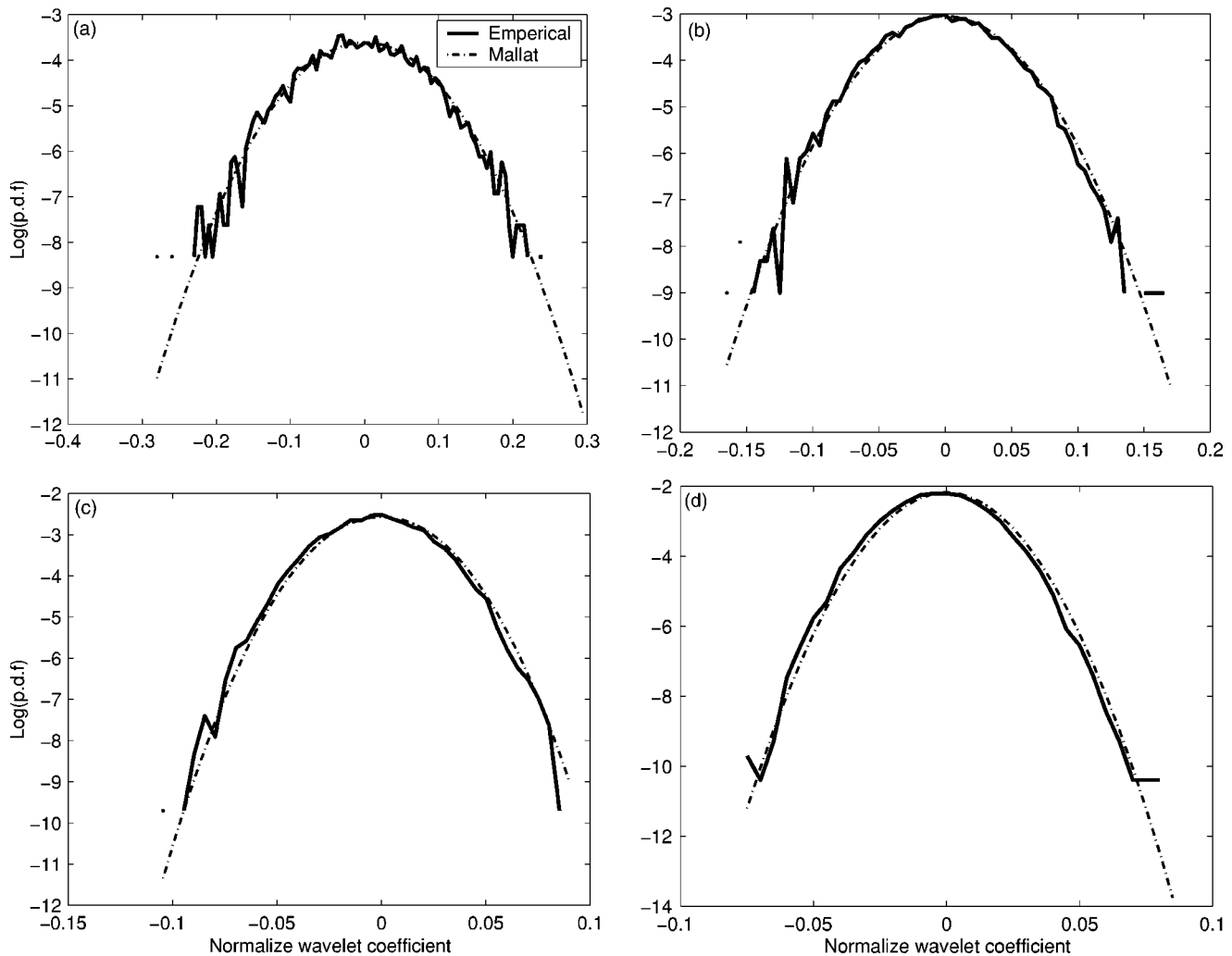


FIG. 2. The logarithms of the empirical density and Mallat's model at different scales for a typical fBm having a Hurst exponent of $1/3$. Four panels show the pdf analysis at the four finest scales in the DWT. The top-left panel is the coarsest scale while the bottom-right panel is the finest scale. The β 's at different scales are estimated from the data and are 1.7891, 1.9388, 1.9307, and 1.9242, respectively. Note that these pdfs are approximately normal.

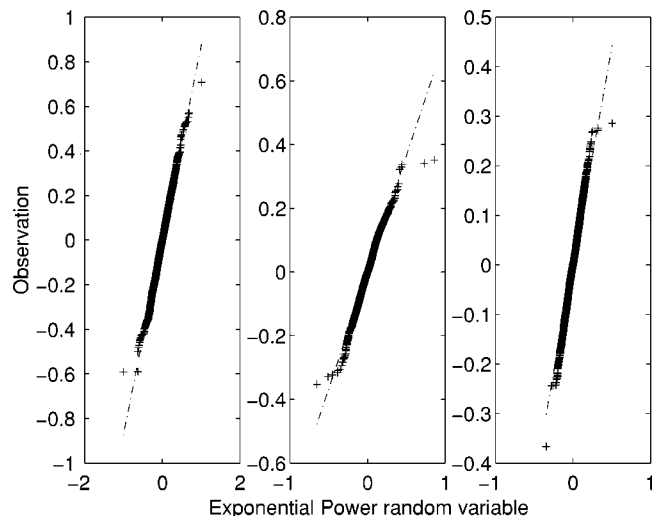


FIG. 3. The $Q-Q$ plots of the measured and modeled random variables at different scales in the wavelet domain for a typical flow variable u . The left panel shows the coarsest scale while the right panel shows the finest scale. The same turbulence measurement time series are used as in Fig. 6.

atmospheric stability itself. That is, a scale index of $j=15$ may not precisely reflect identical eddy sizes for unstable, near-neutral, and stable atmospheric stabilities because of differences in the turbulent intensities (despite equality in mean wind speed). What makes this analysis robust to such a limitation is that the use of orthonormal wavelet transforms means that the scale $j=15$ is not precisely mapped onto one unique frequency or wavenumber (as is the case with Fourier spectra) but a distribution of frequencies (or wavenumbers) set by the wavelet basis. Hence, as long as the relative distortions attributed to the use of Taylor's hypothesis across different stability classes (for the same mean wind) are much smaller than $\ln(2)$, the scale index j may represent the mean eddy sizes across different atmospheric stability regimes. Furthermore, we are restricting this local scalewise analysis

to the three finest scales known to be least affected by distortions due to finite turbulent intensity.

For each of the six runs within each stability class, we fitted the Mallat model for $j=14, 15$, and 16 (out of 16) and all four flow variables. Table III gives the mean and standard errors of the shape parameters for each flow variable and stability class. Unlike the global analysis, we are not able to provide the ANOVA p values since we only have six runs for each regime. This small number of runs makes the statistical inference difficult. As a remedy procedure, we provide the Box plots for these shape coefficients to compare the difference across the stability regimes in Fig. 4. Figure 4 demonstrates that β for all the flow variables, stability regimes, and inertial scales is far from Gaussian ($\beta=2$), and is closer to a double exponential ($\beta=1$). The lowest β (i.e., most heavy tailed) is for temperature at the finest level (irrespective of stability regime). Furthermore, the fastest change in β with scale (i.e., a measure of increased intermittency with decreasing scale) is also for the temperature irrespective of stability class. Hence, the local analysis here clearly demonstrates scalewise dissimilarity between temperature and u within the inertial subrange.

V. DISCUSSION

To explore how atmospheric stability impacts the global scaling properties, we show box plots (Fig. 5) of the quasi-Hurst exponents for all the 95 turbulence measurements.

In the w and T cases the ranges at different stability regimes differ. Their ranges in stable and neutral regimes are totally separated and the median quasi-Hurst values in three regimes are different. Among the three regimes, the median quasi-Hurst values in the stable case tends to be closer to $H=1/3$, which is the theoretical value based on K41. For u and v , it is also noted that the median quasi-Hurst values in the unstable and neutral are very close to each other (i.e., the neutral measurements tend to be similar on average as the

TABLE III. Mean and standard deviation of β 's for all four flow variables and stability classes. Recall that $\beta=2$ for a Gaussian process.

Turbulence	β	u		v		w		Temperature	
		Mean	Standard	Mean	Standard	Mean	Standard	Mean	Standard
$j=16$	Unstable	0.8195	0.0986	0.8912	0.0824	0.8493	0.0731	0.701	0.1715
	Neutral	0.8246	0.074	0.8138	0.1479	0.8296	0.1357	0.6565	0.1127
	Stable	0.9241	0.1124	0.8642	0.0883	0.8183	0.1082	0.6315	0.1573
	All	0.8561	0.1031	0.8564	0.1087	0.8324	0.103	0.663	0.1433
$j=15$	Unstable	0.7204	0.1788	0.8044	0.122	0.7709	0.0804	0.7072	0.157
	Neutral	0.7723	0.1094	0.7196	0.1457	0.7367	0.0845	0.8054	0.234
	Stable	0.9068	0.1831	0.8394	0.173	0.8062	0.161	0.747	0.2365
	All	0.7999	0.1712	0.7878	0.1487	0.7713	0.1117	0.7532	0.2038
$j=14$	Unstable	0.7624	0.2286	0.8978	0.1768	0.7918	0.1356	1.1785	0.3625
	Neutral	0.8636	0.1802	0.8776	0.1404	0.7587	0.0688	1.3546	0.4593
	Stable	0.9563	0.1556	0.8808	0.1949	0.7892	0.0832	1.0551	0.3587
	All	0.8608	0.1967	0.8854	0.162	0.7799	0.0953	1.1961	0.3931

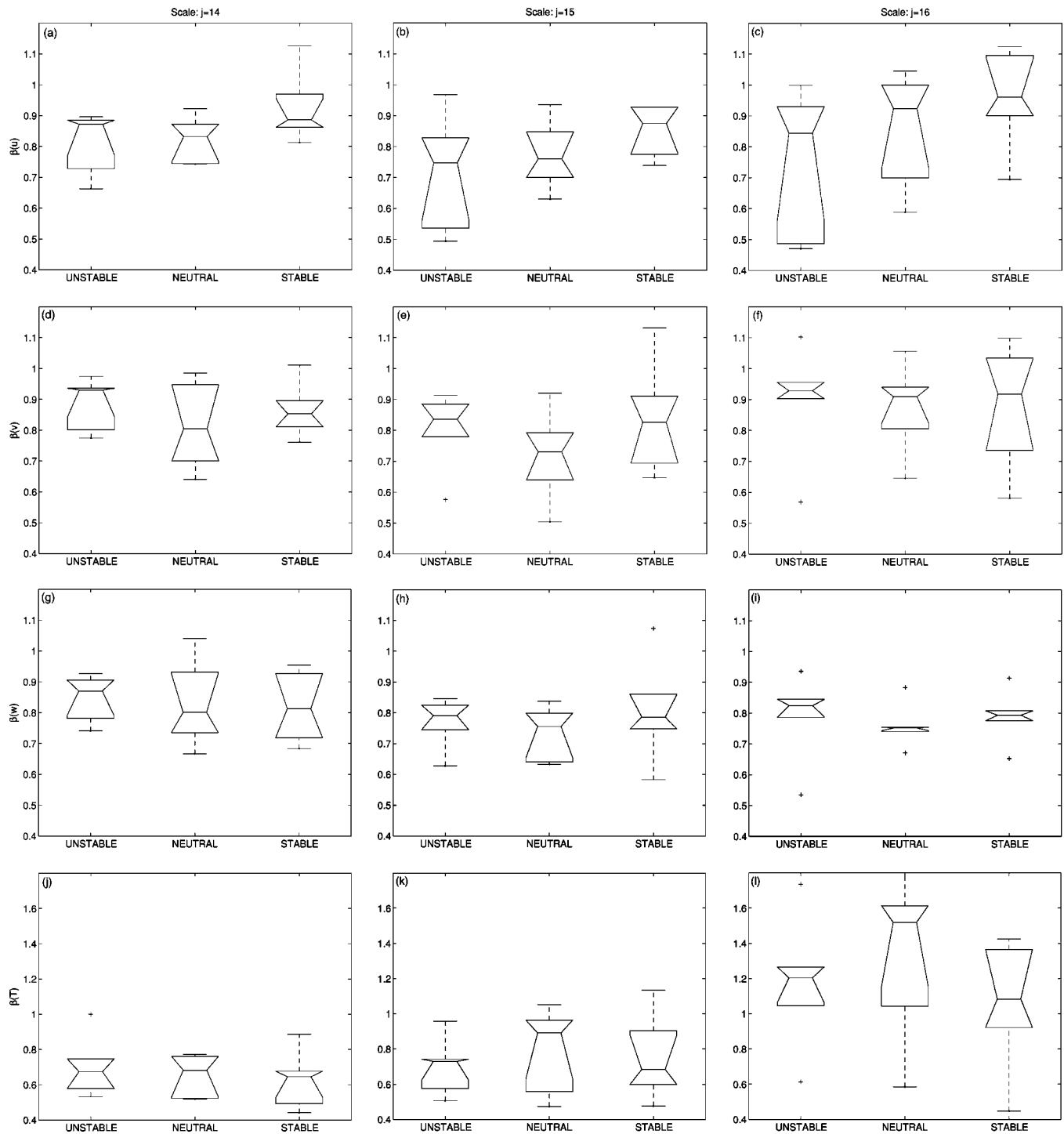


FIG. 4. Box plots of the shape coefficients β in \mathcal{EPD} model across different stability regimes. The four rows correspond to u , v , w , and T , respectively, from the top to the bottom. The three finest scales of wavelet coefficients are used here. The results in the left panels are from the coarsest level ($j=14$) of wavelet decomposition while the right panels refer to the finest level ($j=16$).

unstable ones in terms of the global fractal characteristics), while the those in the stable regime are quite different.

Another important finding is that the ranges of quasi-Hurst exponents in neutral regime are much tighter for u than for the other flow variables. This implies that for neutral atmospheric stability conditions, the global fractal fluctuation of the horizontal velocity is much smaller than for the other variables. Also, the longitudinal velocity is characterized by greater quasi-Hurst exponents in the unstable and neutral re-

gimes than in the stable one, which means that u is more intermittent in the stable regime. The fractal property of u in the stable regime tends to have more global fractal fluctuation than in unstable regime because the quasi-Hurst range is broader. However, this pattern seems opposite in the lateral velocity. This difference may be attributed to random shifts in wind direction. As an almost common phenomena for u , v , and T , their quasi-Hurst values are generally larger than $H = 1/3$. However, the quasi-Hurst values of w is overall

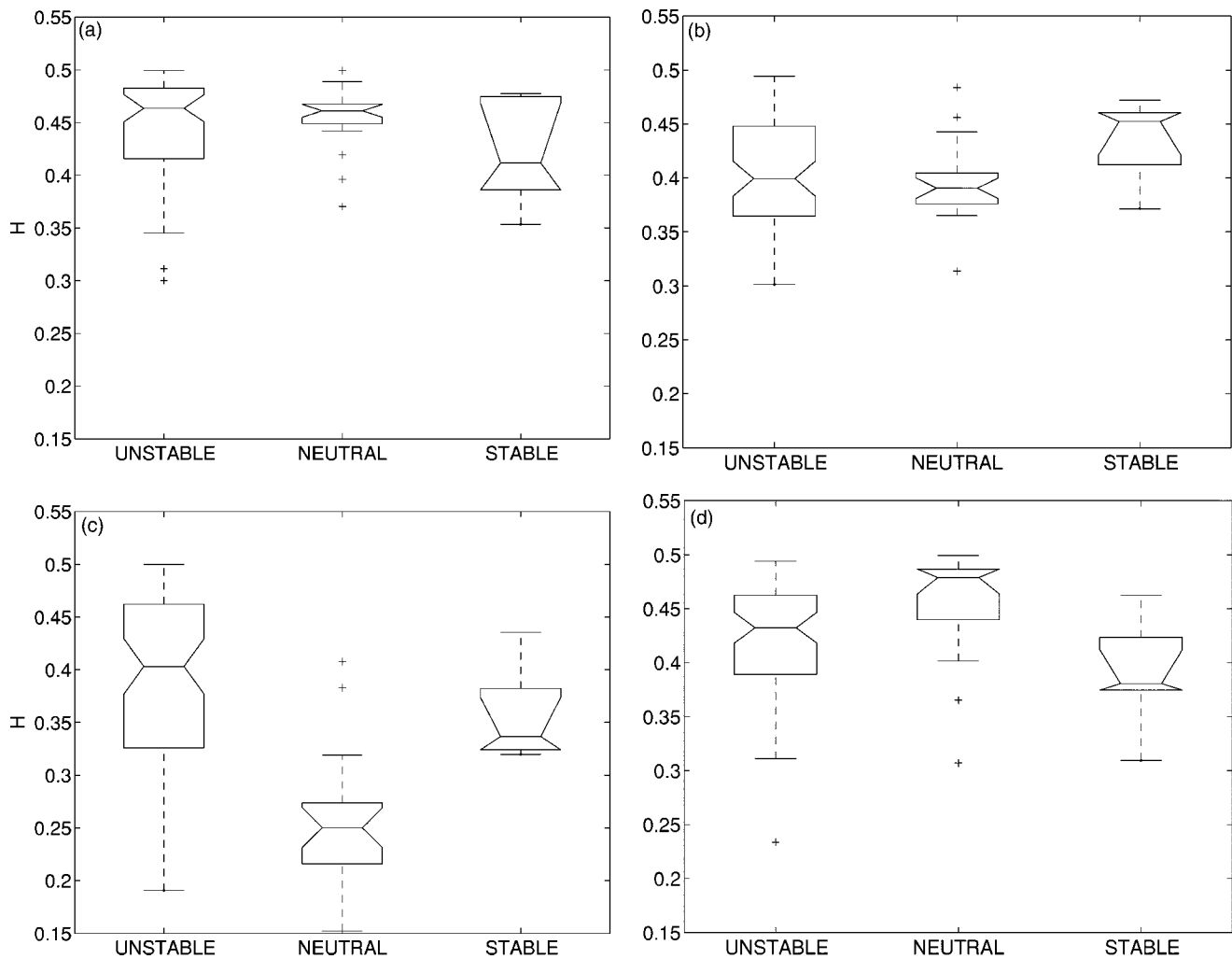


FIG. 5. Box plots of the quasi-Hurst exponents \hat{H} for four flow variables u , v , w , and T from the top left to the bottom right, respectively.

smaller than the other three flow variables, and, interestingly, the quasi-Hurst values in the neutral are much smaller.

The scalewise comparison provides complementary evidence for the above arguments. The “average” pdfs (in Mallat’s model) associated with atmospheric stability conditions of the four flow variables at the three finest scales are computed. To obtain such pdfs, we averaged the estimated parameters (including both the shape parameters and scale parameters) within a stability regime and use these averages as new parameters to specify the scalewise pdfs for each flow variable (see Fig. 6). The plots in Fig. 6 suggest that u , v , and T appear to be sensitive to atmospheric stability while w is not. The results here suggest that the local scaling parameters are more sensitive to the effects of atmospheric stability than the global scaling parameters.

VI. CONCLUSIONS

This study assessed the effects of atmospheric stability on the inertial subrange structure of u , v , w , and T using both local and global measures in the wavelet domain. The global measure relied on a quasi-Hurst exponent calculation while the local measure was based on the Tsallis thermostatistic

entropy approach shown to be analogous to $\mathcal{EPD}(\alpha, \beta)$ family. The analysis here demonstrated the following.

(i) Both $\mathcal{EPD}(\alpha, \beta)$ and the Tsallis thermostatistic entropy approach reproduces reasonably well the scalewise velocity and temperature properties within the inertial subrange and for all stability classes, consistent with several recent studies.

(ii) The scalewise analysis demonstrates that the distributional properties of the velocity and temperature within the inertial subrange are far from Gaussian and with tails even heavier than a double exponential for all stability classes.

(iii) The local or scalewise analysis clearly identified dissimilarities between temperature and velocity even within the same stability class.

(iv) The global measures were less sensitive to atmospheric stability than the scalewise measures. In particular, the global measure identified the T and w components as the only flow variables whose inertial subrange has been statistically impacted by atmospheric stability. On the other hand, atmospheric stability clearly impacted the parameters of $\mathcal{EPD}(\alpha, \beta)$ for u , v , and T . This analysis is in agreement with an earlier analysis by Katul *et al.* (Ref. 29) who dem-

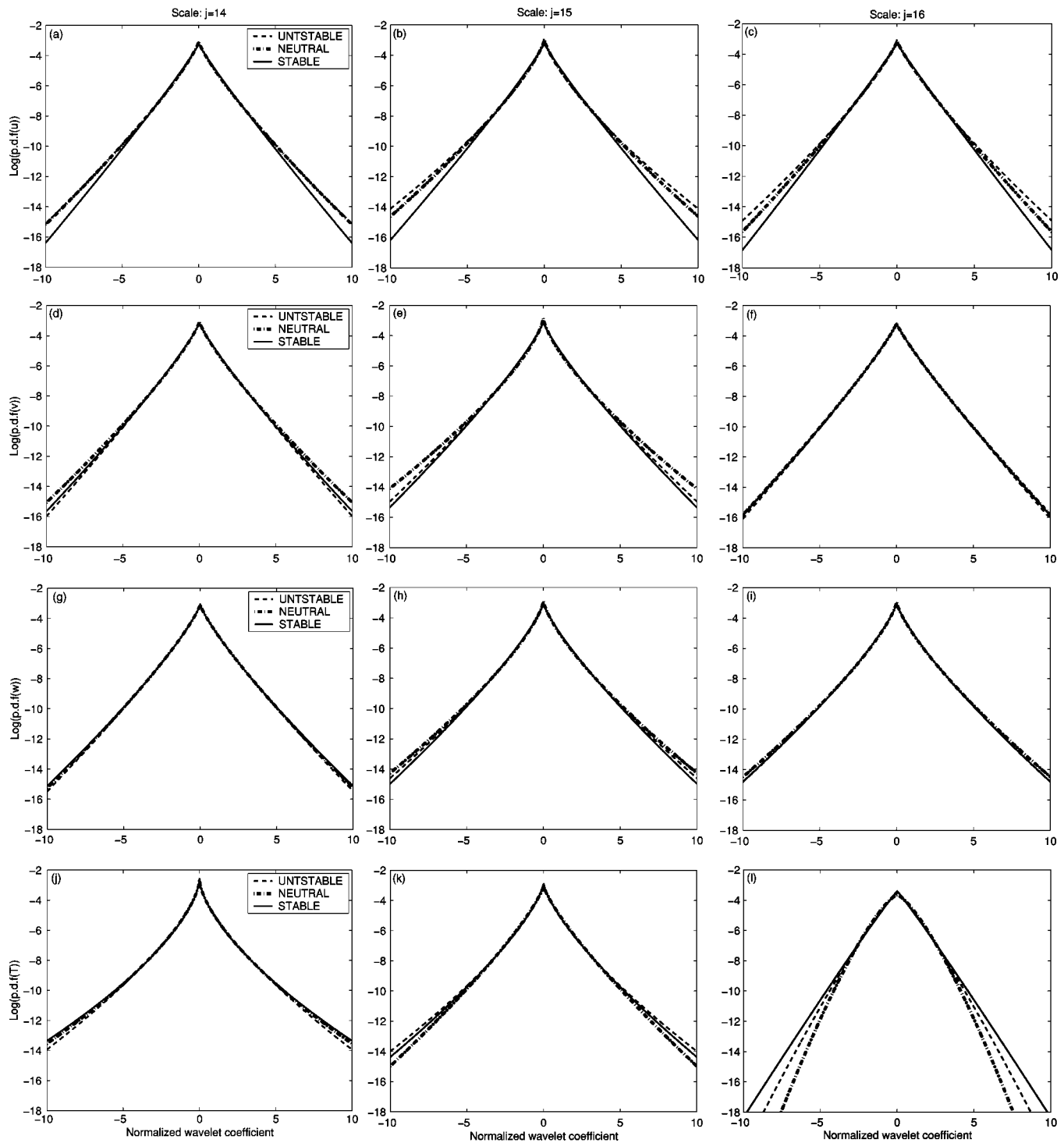


FIG. 6. The average logarithm pdfs associated with atmospheric stability conditions of the four flow variables (u, v, w, T) at first three finest scales. The four rows are corresponding to measurement u, v, w , and T , respectively from the top to the bottom. Three finest scales of wavelet coefficients are used here. The results in the left panels are from the coarsest level ($j=14$) of wavelet coefficients while the right panels refer to the finest level ($j=16$).

onstrated, via a functional ANOVA (FANOVA), that atmospheric stability impacts the wavelet-based multifractal spectrum of u, v , and T .

When conclusions (iii) and (iv) are taken together, it is clear that the inertial subrange of temperature is unambiguously impacted by atmospheric stability—both locally and globally. This analysis lends some support to the conclusions

by Shraiman and Siggia⁵ who suggested that the statistical properties of “scalar” turbulence are decoupled from those of the underlying velocity. That is, the added complexity in scalar turbulence (e.g., here added complexity refers to greater intermittency and overall sensitivity to boundary conditions) is not derived from the complexity in the velocity field, but also from the mixing process itself, and boundary conditions

(or injection of energy). Finally, we note that the symbiotic use of global and local scaling analysis proposed here lends further confidence in the validity of the above conclusion for T .

ACKNOWLEDGMENTS

This project was supported by the National Science Foundation (Grants No. EAR-0208258, No. DMS-0072585, and No. NSA-24-60R). The experiments are part of a long-term CO₂ flux monitoring initiative supported by the Office of Science (BER), U.S. Department of Energy, Cooperative Agreement No. DE-FC02-03ER63613.

APPENDIX: $\mathcal{E}PD$ DISTRIBUTION AS TSALLIS MAXENT SOLUTION

The traditional entropy theory is based on Shannon's definition; more general measures, such as Renyi and Tsallis (sometimes called Tsallis–Havrda–Charvat, or Havrda–Charvat entropy, since the definition of this entropy measure was first given in Ref. 30) have also been proposed. Practical applications and theoretical implications of Tsallis-type entropy are active research areas in the physical sciences, especially turbulence.^{23,31–35}

For example, *Tsallis thermostatistic* is based on Tsallis entropy which is a generalization of the Shannon (Boltzmann–Gibbs) entropy. The Tsallis entropy^{36,37} is given by

$$S_q = \frac{1}{q-1} \left(1 - \int_{-\infty}^{\infty} p(x)^q dx \right), \quad (\text{A1})$$

where $p(x)$ is the probability density of the microstate x of the system (in our case, the microstate refers to the individual velocity of the turbulence) and q is the nonextensive parameter (also regarded as a measure of the information incompleteness). The ordinary Shannon entropy is obtained as a special case when $q \rightarrow 1$. Tsallis' measure of entropy is more flexible than Shannon's due to its adaptive parametrization. We find that the Maxent (maximum-entropy) probability distribution of a random variable X representing the turbulent measurements is constrained as follows:

$$\int_{-\infty}^{\infty} p(x) dx = 1 \quad (\text{A2})$$

and

$$\int_{-\infty}^{\infty} p(x) \epsilon_x dx = E, \quad (\text{A3})$$

where E is the energy content of x and should be a known constant, and ϵ_x 's denote the energies at various microstates. The exact definition of ϵ_x in reality depends on the condition of the flow; roughly it can be taken as $\epsilon_x = x^2/2$ (x is assumed to be the velocity at this microstate). The general maximizing solution or Maxent distribution has the following form:³⁸

$$p(x) = \frac{1}{K_q} [1 + (q-1)\beta_1 \epsilon_x]^{1/(1-q)}, \quad (\text{A4})$$

where

$$K_q = \int_{-\infty}^{\infty} [1 + (q-1)\beta_1 \epsilon_x]^{1/(1-q)} dx \quad (\text{A5})$$

is the so-called partition function and $\beta_1 = 2/(5-3q)$ is a suitable inverse *temperature-like* variable. Interestingly, the value of q can be related to the properties of the Maxent distribution as follows.

If $1 < q < 3$, we could evaluate (A5) with $\epsilon_x = x^2/2$ as

$$\begin{aligned} K_q &= \int_{-\infty}^{\infty} \left[1 + \frac{1}{2}(q-1)\beta_1 x^2 \right]^{1/(1-q)} dx \\ &= \left[\frac{\pi}{\beta_1(q-1)} \right]^{0.5} \frac{\Gamma[1/(q-1) - 1/2]}{\Gamma[1/(q-1)]}, \end{aligned} \quad (\text{A6})$$

where $\Gamma(\cdot)$ represents the standard Gamma function. Furthermore, the second moment is calculated when $1 < q < 5/3$ as

$$EX^2 = \frac{2}{\beta_1(5-3q)}. \quad (\text{A7})$$

However, this second moment tends to infinity if $q \geq 5/3$ and the so-called heavy-tailed distribution, which is universally recognized as a basic characteristic of turbulence, is recovered in this case.

If $q > 3$, the integral defining K_q would diverge and hence the probability density function does not exist.

If $q \rightarrow 1$, the distribution in (A4) converges to normal.

If $q < 1$, the distribution in (A4) would resemble a cutoff distribution. Below, we briefly explore further links between Mallat's model and the Tsallis Maxent model.

Comparison of canonical forms of Mallat's and Tsallis models indicate close relationship between the $\mathcal{E}PD$ family and the Maxent distribution. Both of them include the uniform, normal, and Laplace distributions as special cases, as well as an infinite number of distributions with arbitrary variances and kurtosis. We demonstrate this link empirically using turbulent velocity time series. First, the turbulence time series is decomposed into three successive finest scales using discrete wavelet transformation. These scales are within the inertial subrange as discussed in Ref. 28. We utilize the Daubechies four-tap filter to ensure a balance of localization in time and frequency domains (i.e., a compromise between the Haar and Fourier bases). Next, we estimate the nonextensive parameter q for each scale using the relationship between q and the moments,

$$EX^m = \frac{1}{2^m} \prod_{j=0}^{m-1} \frac{5+2j}{4+j-(3+j)q}, \quad (\text{A8})$$

where X is a Maxent distributed random variable. To give an estimator of q , we utilize the kurtosis κ , which is usually defined as

$$\kappa = \frac{EX^4}{(EX^2)^2}. \quad (\text{A9})$$

We substitute the expressions for EX^4 and EX^2 evaluated by (A8) and solve (A9) with respect to q . The solution is

$$q = \frac{7\kappa - 15}{5\kappa - 9}. \quad (\text{A10})$$

Once the parameter q is evaluated, the complete form of the normalized Tsallis Maxent distribution of unit variance, which is assumed to be the theoretical distribution of wavelet coefficients, is specified. The empirical pdfs of the scalewise wavelet coefficients are compared with the corresponding Tsallis Maxent distribution in Fig. 2. In addition, we also fit Mallat's model for the scalewise coefficients. For simplicity, the variances of these scalewise coefficients have been normalized to unity.

The results shown in Fig. 2 suggest an almost perfect match among these three types of pdfs, especially at the tails. The large departures from the measured pdf around the center points is attributed to the "zoom effect" of logarithmic representation. The turbulence data we analyzed in Fig. 2 is for a longitudinal velocity run collected in stable atmospheric conditions. The pdfs of wavelet coefficients for the other flow variables v , w , and T and for different stability regimes behave similarly as those in Fig. 2. We conclude that the marginal distribution of the turbulence wavelet coefficients at a fixed scale well match the maximum Tsallis entropy distribution. At the same time, the \mathcal{EPD} model also fits well the empirical pdf. This empirical closeness demonstrates the inherent link between the \mathcal{EPD} and the Tsallis Maxent distribution, explored next.

It is demonstrated that the Maxent solution is the marginal likelihood obtained from the \mathcal{EPD} (α, β) model when the prior on β is the inverse Γ . In other words, the Maxent solution is the scale mixture of \mathcal{EPD} distributions with the inverse Γ as mixing distribution.

Consider a random variable X distributed as the exponential power family with conditional pdf given by

$$f(x|\alpha, \beta) = K \exp(-(|x|/\alpha)^\beta). \quad (\text{A11})$$

Under the Bayesian paradigm, the scale parameter α is considered random and given a prior distribution. The marginal likelihood distribution of X given β is then obtained by integrating out α . Assume that $\lambda = \alpha^{-1}$ has prior distribution $\Gamma[n/2, n/(2\lambda_0)]$ with density,

$$g(\lambda) = \frac{1}{\Gamma\left(\frac{n}{2}\right)} \left(\frac{n}{2\lambda_0}\right)^{n/2} \lambda^{(2/n)-1} \exp\left\{-\frac{n\lambda}{2\lambda_0}\right\}, \quad (\text{A12})$$

with $\lambda_0 = E(\lambda)$.

Combining (A11) and (A12) we have

$$f(x|\beta) = \int_{-\infty}^{\infty} f(x|1/\lambda, \beta) g(\lambda) d\lambda. \quad (\text{A13})$$

There exists a closed form solution of this integral given by

$$f(x|\beta) = \frac{1}{K_q} [1 + (q-1)\lambda_1|x|^\beta]^{1/(1-q)}, \quad (\text{A14})$$

where

$$q = 1 + \beta/(\beta n/2 + 1), \quad (\text{A15})$$

$$\lambda_1 = \frac{\beta}{1 + \beta - q} \lambda_0, \quad (\text{A16})$$

and

$$K_q = \int_{-\infty}^{\infty} (1 + (q-1)\lambda_1|x|^\beta)^{1/(1-q)} dx. \quad (\text{A17})$$

Hence, when the shape parameter is assumed from a particular prior, the marginal likelihood obtained from the model \mathcal{EPD} in a Bayesian fashion is the maximum Tsallis entropy solution.

- ¹J. Someria, "Unweaving the whirls," *Nature (London)* **413**, 575 (2001).
- ²U. Frisch, *Turbulence* (Cambridge University Press, Cambridge, 1995), p. 296.
- ³K. R. Sreenivasan and R. A. Antonia, "The phenomenology of small scale turbulence," *Annu. Rev. Fluid Mech.* **29**, 435 (1997).
- ⁴U. Frisch, A. Mazzino, and M. Vergassola, "Intermittency in passive scalar advection," *Phys. Rev. Lett.* **80**, 5532 (1998).
- ⁵B. I. Schraiman and E. D. Siggia, "Scalar turbulence," *Nature (London)* **405**, 439 (2000).
- ⁶L. Biferale and M. Vergassola, "Isotropy vs anisotropy in small-scale turbulence," *Phys. Fluids* **13**, 2139 (2001).
- ⁷Z. Warhaft, "Passive scalars in turbulent flows," *Annu. Rev. Fluid Mech.* **32**, 203 (2000).
- ⁸A. N. Kolmogorov, "Local structure of turbulence in an incompressible fluid for very large Reynolds numbers," *Dokl. Akad. Nauk SSSR* **30**, 299 (1941).
- ⁹A. N. Kolmogorov, "A refinement of previous hypotheses concerning the local structure of turbulence in a viscous incompressible fluid at high Reynolds number," *J. Fluid Mech.* **13**, 82 (1962).
- ¹⁰A. Pumir and B. I. Schraiman, "Persistent small scale anisotropy in homogeneous shear flows," *Phys. Rev. Lett.* **75**, 3114 (1995).
- ¹¹A. Celani, A. Lanotte, A. Mazzino, and M. Vergassola, "Universality and saturation of intermittency in passive scalar turbulence," *Phys. Rev. Lett.* **84**, 2358 (2000).
- ¹²N. V. Antonov and J. Honkonen, "Anomalous scaling in two models of passive scalar advection: Effects of anisotropy and compressibility," *Phys. Rev. E* **63**, 036302 (2001).
- ¹³J. D. Albertson, G. G. Katul, M. B. Parlange, and W. E. Eichenger, "Spectral scaling of static pressure fluctuations in the atmospheric surface layer: The interaction between large and small scales," *Phys. Fluids* **10**, 1725 (1998).
- ¹⁴A. Celani and M. Vergassola, "Statistical geometry in scalar turbulence," *Phys. Rev. Lett.* **86**, 424 (2001).
- ¹⁵J. Qian, "Inertial range and the finite Reynolds number effect of turbulence," *Phys. Rev. E* **55**, 337 (1997).
- ¹⁶J. Qian, "Slow decay of the finite Reynolds number effect of turbulence," *Phys. Rev. E* **60**, 3409 (1999).
- ¹⁷Y. Gagne, B. Castaing, C. Baudet, and Y. Malécot, "Reynolds dependence of third-order velocity structure functions," *Phys. Fluids* **16**, 482 (2004).
- ¹⁸G. G. Katul, C. I. Hsieh, and J. Sigmon, "Energy-inertial scale interaction for temperature and velocity in the unstable surface layer," *Boundary-Layer Meteorol.* **82**, 49 (1997).
- ¹⁹G. G. Katul, B. Vidakovic, and J. D. Albertson, "Estimating global and local scaling exponents in turbulent flows using wavelet transformations," *Phys. Fluids* **13**, 241 (2001).
- ²⁰H. E. Hurst, "Long-term storage capacity of reservoirs," *Proc. Am. Soc. Civ. Eng.* **76**, 11 (1950).
- ²¹J. F. Coeurjolly, "Simulation and identification of the fractional Brownian motion: a bibliographical and comparative study," *J. Stat. Software* **5**, 7 (2000).
- ²²S. G. Mallat, "A theory for multiresolution signal decomposition: the wave-

- let representation," IEEE Trans. Pattern Anal. Mach. Intell. **11**, 674 (1989).
- ²³C. Beck, "Generalized statistical mechanics and fully developed turbulence," Physica A **306**, 189 (2002).
- ²⁴Z. She and E. Leveque, "Universal scaling laws in fully developed turbulence," Phys. Rev. Lett. **72**, 336 (1994).
- ²⁵K. Aivalis, K. Sreenivasan, Y. Tsuji, J. Klewicki, and C. Biltoft, "Temperature structure functions for air flow over moderately heated ground," Phys. Fluids **14**, 2439 (2002).
- ²⁶G. Katul and M. Parlange, "On the active role of temperature in surface layer turbulence," J. Atmos. Sci. **51**, 2181 (1994).
- ²⁷G. G. Katul, C. I. Hsieh, and J. Sigmon, "Energy-inertial scale interaction for temperature and velocity in the unstable surface layer," Boundary-Layer Meteorol. **82**, 49 (1997).
- ²⁸G. G. Katul, C. T. Lai, J. D. Albertson, B. Vidakovic, K. Schafer, C. I. Hsieh, and R. Oren, "Quantifying the complexity in mapping energy inputs and hydrologic state variables into land-surface fluxes," Geophys. Res. Lett. **28**, 3305 (2001).
- ²⁹G. G. Katul, C. Angelini, D. D. Cantitiis, U. Amato, B. Vidakovic, and J. Albertson, "Are the effects of large scale flow conditions really lost through the turbulent cascade?" Geophys. Res. Lett. **29**, 13-1 (2003).
- ³⁰M. E. Havrda and F. Charvat, "Quantification method of classification processes: Concept of structural α -entropy," Kybernetika **3**, 30 (1967).
- ³¹C. Beck, "On the small-scale statistics of Lagrangian turbulence," Physica A **287**, 240 (2001).
- ³²T. Arimitsu and N. Arimitsu, "Analysis of fully developed turbulence in terms of Tsallis statistics," Phys. Rev. E **61**, 3237 (2000).
- ³³T. Arimitsu and N. Arimitsu, "Tsallis statistics and turbulence," Chaos, Solitons Fractals **13**, 149 (2002).
- ³⁴T. Arimitsu and N. Arimitsu, "PDF of velocity fluctuation in turbulence by a statistics based on generalized entropy," Physica A **305**, 218 (2002).
- ³⁵F. M. Ramosa, R. R. Rosaa, C. R. Netoa *et al.*, "Non-extensive statistics and three-dimensional fully developed turbulence," Physica A **295**, 250 (2001).
- ³⁶C. Tsallis, "Possible generalization of Boltzmann-Gibbs statistics," J. Stat. Phys. **52**, 479 (1988).
- ³⁷C. Tsallis, R. S. Mendes, and A. R. Plastino, "The role of constraints within generalized nonextensive statistics," Physica A **261**, 534 (1998).
- ³⁸D. Prato and C. Tsallis, "Nonextensive foundation of Levy distributions," Phys. Rev. E **60**, 2398 (1999).